Intramolecular Charge-Transfer Excited-State Processes in 4-(*N,N*-Dimethylamino)benzonitrile: The Role of Twisting and the $\pi\sigma^*$ State

Ivelina Georgieva,*[†] Adélia J. A. Aquino,[‡,§] Felix Plasser,[§] Natasha Trendafilova,[†] Andreas Köhn,[||] and Hans Lischka*[‡,§]

[†]Institute of General and Inorganic Chemistry, Bulgarian Academy of Sciences, Sofia, Bulgaria

[‡]Department of Chemistry and Biochemistry, Texas Tech University, Lubbock, Texas 79409-1061, United States

[§]Institute for Theoretical Chemistry, University of Vienna, A-1090 Vienna, Austria

[||]Institute for Theoretical Chemistry, University of Stuttgart, 70569 Stuttgart, Germany

ⓈSupporting Information

ABSTRACT: The structural processes leading to dual fluorescence of 4-(dimethylamino)benzonitrile in the gas phase and in acetonitrile solvent were investigated using a combination of multireference configuration interaction (MRCI) and the second-order algebraic diagrammatic construction (ADC(2)) methods. Solvent effects were included on the basis of the conductor-like screening model. The MRCI method was used for computing the nonadiabatic interaction between the two lowest excited $\pi\pi^*$ states ($S_2(L_a$, CT) and $S_1(L_b$, LE)) and the corresponding minimum on the crossing seam (MXS) whereas the ADC(2) calculations were dedicated to assessing the role of the $\pi\sigma^*$ state. The MXS structure was found to have a twisting angle of ~50°. The branching space does not contain the twisting motion of the dimethylamino group and thus is not directly involved in the deactivation process from S_2 to S_1. Polar solvent effects are not found to have a significant influence on this situation. Applying C_s symmetry restrictions, the ADC(2) calculations show that CCN bending leads to a strong stabilization and to significant charge transfer (CT). Nevertheless, this structure is not a minimum but converts to the local excitation (LE) structure on releasing the symmetry constraint. These findings suggest that the main role in the dynamics is played by the nonadiabatic interaction of the LE and CT states and that the main source for the dual fluorescence is the twisted internal charge-transfer state in addition to the LE state.
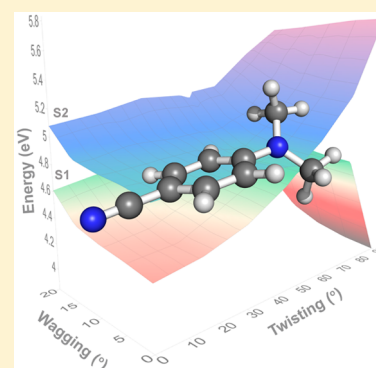
INTRODUCTION

The investigation of intramolecular charge transfer (ICT) in donor–acceptor systems such as substituted benzenes reveals many interesting processes occurring in electronically excited states. Particularly, dual fluorescence of 4-(*N,N*-dimethylamino)benzonitrile (DMABN) in polar solution, consisting of an emission from the ^1L_b state and an "anomalous" red-shifted emission from the ^1L_a state[1] has attracted considerable attention. The ^1L_b state is usually characterized to be local excitation (LE) and the ^1L_a state as charge-transfer (CT) state. The position and intensity of the red-shifted band show a marked dependence on solvent polarity. This property was interpreted as an indication for a large dipole moment of the emitting state and hence for its charge-transfer character. In contrast to solution, in the gas phase, the emission spectrum of DMABN consists of a single local excitation (LE) fluorescence band $S_1(^1L_b)$, and evidence for a LE → ICT process in DMABN was not found.[2,3] The structural and electronic nature of the red-shifted emission band of DMABN has been explained by means of several excited-state ICT mechanisms. The most widely accepted concept is based on the twisted

intramolecular charge-transfer (TICT)[4−6] model in which the torsion of the dimethylamino group around the CN bond to the phenyl ring induces a charge transfer in which the former group acts as electron donor and the benzonitrile moiety as the electron acceptor. Alternatively, a CT process has been suggested to occur at planar DMABN structures (PICT model) where the vibronic interaction in the Franck–Condon region is the important factor for the formation of the CT state.[3,7] The third model to be mentioned here is the rehybridized ICT (RICT) model[8,9] representing a bent $\pi\sigma^*_{CN}$ state. Even though it was not considered a viable alternative to the TICT model for DMABN originally, in later work[10] the main features have been taken up as the origin of a new state involved in the electron-transfer dynamics.[11]

Based on the models listed above, the structural and dynamical aspects of the ICT in DMABN have been widely investigated from an experimental[1−6,12−22] as well as from a

computational point of view.[10,23−42] The absorption spectrum of DMABN in the gas phase consists of a main band with a maximum at 4.57 eV attributed to $S_2(L_a,CT)$ and a weak absorption with a lower-energy shoulder with a band maximum given at 4.13 eV attributed to the $S_1(L_b, LE)$ state.[2,3,43] The ultrafast photodynamics of DMABN starting in the bright $S_2(^1L_a)$ state has been investigated by Fuss et al.[18,44] by means of femtosecond pump−probe experiments in the gas phase using nonresonant multiphoton ionization as a probe process. The main mechanistic result deduced from this investigation is the ultrafast relaxation (68 fs) to the CT and L_b-type S_1 states. After equilibration within 1 ps, the molecule relaxes further within 90 ps to a lower excited triplet state and then decomposes within 300 ps. It was also shown that the passage through the conical intersection involves strong geometrical distortions which were related to a twist coordinate. Fluorescence excitation spectra of jet-cooled DMABN studied by Salgado et al.[45] led to a similar analysis of the photodynamics indicating also a broadening of the rotational contour above an excess energy of 600 cm^{-1}. This fact was ascribed in ref 18 to the conversion of the initially excited L_b state to the higher-lying CT state with an activation barrier of 600 cm^{-1}.

Quantum chemical calculations exploring the torsional potential within the TICT model performed at configuration interaction with singles (CIS), complete active space self-consistent field (CASSCF), and CAS perturbation theory to second order (CASPT2) by Sobolewski et al.[10] show that the former two methods do not provide a correct description of the torsional behavior of the LE and CT states, e.g., the CASSCF approach does not lead to a crossing between the two states at ~45°. CASPT2 calculations have been also performed by Serrano-Andres et al.[23] In this work, the effect of the torsional mode in the TICT model and the wagging mode of the dimethylamino group have been compared with respect to the charge transfer required by the dependence of the second fluorescence band on polar solvents. It was shown that in contrast to the torsional mode, the wagging mode was unable to lead to the required significant charge separation, thus favoring the TICT model for the explanation of the experimental findings. A similar conclusion has been reached by Mennucci et al.[33] based on multireference perturbation configuration interaction (CIPSI). Full geometry optimizations of the LE and CT states have been reported by Rappoport and Furche[26] based on time-dependent density functional theory (TD-DFT) and by Köhn and Hättig[27] using the approximate coupled-cluster singles-and-doubles method CC2. Both studies also investigate the change in force constants and vibrational frequencies of the LE and CT states as compared to the ground state and find good agreement with picosecond time-resolved infrared (IR) and resonance Raman spectra.[15−17,46] According to these studies, the LE state has a C_2 symmetric minimum. In the CC2 calculations, three coordinates contribute to the reaction path from LE to ICT: the twisting motion of the dimethylamino group, the just-mentioned pyramidalization of the ring carbon atom, and quinoidalization modes of the ring. Both TD-DFT and CC2 support the assumption that the torsional mode stabilizes the CT state and is a major driving force of the photodynamics.

The investigation by Gómez et al.[29] was dedicated to the description of the S_2/S_1 intersection seam and its connection to the internal conversion process. It was found that the torsion of the $N(CH_3)_2$ group is not included in the two coordinates

describing the intersection seam. Thus, the S_2/S_1 degeneracy is conserved along the amino-group torsion. Two pathways were discussed in this work. The first consists of a nonadiabatic reaction path, evolving after vertical excitation to S_2 via the transient S_2-PICT structure toward the crossing seam. Depending on the actual torsional angle, a wide range of the seam can be accessed where internal conversion to S_1 can occur. On the basis of the fact that the minimum of the intersection seam has a planar structure, the formation of the S_1-LE state is expected to be preferred. The other pathway possesses adiabatic character and connects the LE and TICT structures on the S_1 state with an energy barrier of 18 kcal/mol from the side of the LE structure. Recent nonadiabatic photodynamics simulations[42] based on the algebraic diagrammatic construction method to second order (ADC(2))[47,48] show a picture which is in good agreement with the findings of Gómez et al.[29] The transition from the S_2 to the S_1 state is extremely fast (8.5 fs) and does not include the $N(CH_3)_2$ twisting motion. Population of the TICT state occurs primarily via equilibration from the LE state as already suggested in ref 22 based on time-correlated single-photon counting experiments.

The idea of the RICT structure has been taken up in TDDFT/BP86 calculation by Zgierski and Lim.[11] By variation of the C(Ph)CN angle in DMABN, a $1^1A''(\pi\sigma^*)$ state is found, located at ~120° and 3.28 eV above the ground state. This state is characterized by the charge transfer from an aromatic π orbital to a σ^* orbital of the cyano group. Subsequent TDDFT/B3LYP calculations[36] resulted in an energy of 4.20 eV for that state, a value which compares somewhat better with CASPT2 results of 4.50 eV[10,36] and 4.92 eV.[38]

Transient excited-state absorption (ESA) of DMABN measured in n-hexane and in acetonitrile[49] (AN) plays an important part in analyzing the role of the ICT for the dual fluorescence mechanism. In hexane, a uniform decrease of all absorption bands is observed and no indication for an ICT state is found. In acetonitrile, the situation is different. A decrease of the bands at 360 and ~680 nm assigned to LE absorption combined with an increase of the ICT band at 320 nm is found. Both the appearance of the ICT band and the decrease of the bands assigned to the LE state occur with the same lifetime of 4 ps. The character of the 680 nm band has been reassigned to a $\pi\sigma^*-\pi\sigma^*$ transition[36] based on the absence of $\pi\pi^*$ transitions with significant oscillator strength starting from the L_b state computed at the TDDFT level and the observed blue shift of the 680 nm band with increasing probe delay times. The latter observation compares well with the charge-transfer character of the $\pi\sigma^*$ state. The just-mentioned reassignment led to the proposition of a $\pi\sigma^*$-mediated ICT mechanism where a reaction sequence of $\pi\pi^* \rightarrow \pi\sigma^* \rightarrow$ ICT structures is proposed.[36] However, it should be mentioned that CASPT2 calculations were reported[50] which, in contrast to the just-mentioned TDDFT investigations, give excitation energies for the LE state which are in good agreement with the experimentally observed bands so that from that point of view a $\pi\sigma^*$ state need not be invoked for the assignment of the 680 nm band.

The differences in the nanosecond decay time between the transient absorption of the TICT state (~4.8 ns) and the fluorescence decay of the ICT (2.9 ns)[37,38] in AN led to the conclusion that these two states are not identical. Combined CASSCF and CASPT2 calculations reported in ref 38 indicated the existence of a partially twisted ICT (pTICT) structure with a twisting angle of 53°. The fluorescence with the decay time of
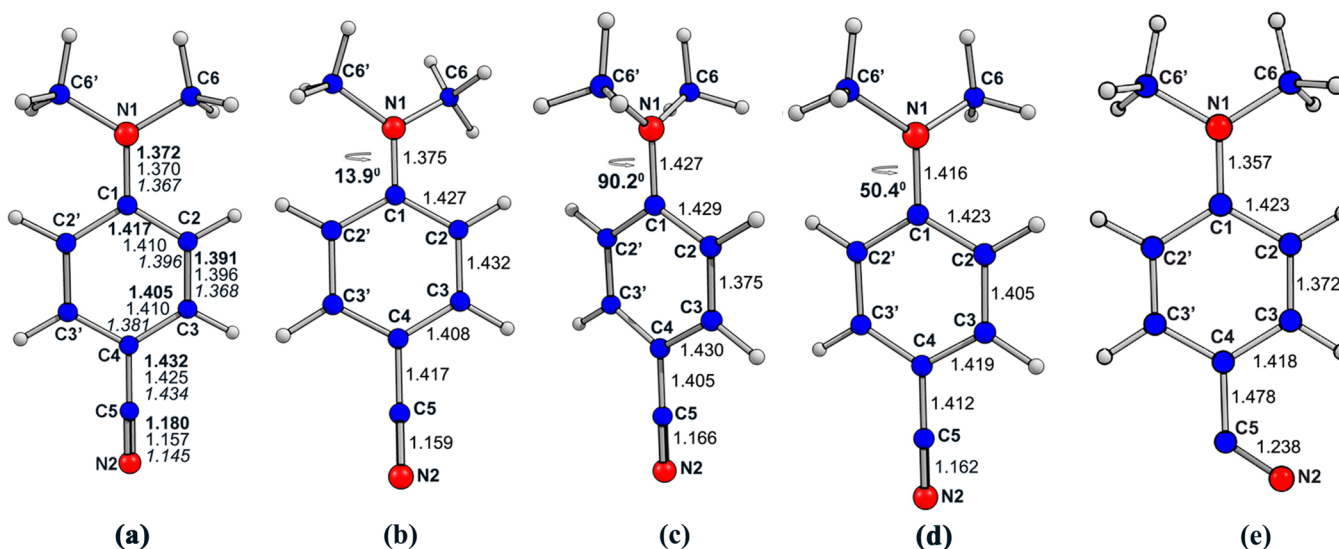
Figure 1. Optimized geometries of DMABN in the ground state (C_{2v} symmetry) (a), in the S_1(LE) state (C_2) (b), in the CT state (C_1) (c), in the S_2/S_1 MXS (C_2) (d) at the MRCIS (8,7)/ANO-DZ level, and in the $\pi\sigma^*$ state (C_s) (e) at the ADC(2)/TZVP level. For the ground-state structure, the MRCIS (8,7)/ANO-DZ results are given in roman type, MP2/SVP data are presented in bold, and the experimental data in italic.

2.9 ns was uniquely assigned to originate from the pTICT structure.

In view of the still existing different interpretations and structural models for the explanation of the dual fluorescence of DMABN, the purpose of the present study is to perform a detailed survey of the excited-state mechanism of ICT using multireference methods[51] which can simultaneously describe the energy surfaces of the LE and CT states and their nonadiabatic crossing regions and are capable of full optimization of excited-state geometries and conical intersections. Special emphasis is given to the calculation of solvent effects in the excited state using a polarizable continuum model based on the conductor-like screening model (COSMO).[52] Acetonitrile has been chosen as a solvent because of available experimental data. The question of dual fluorescence of DMABN in that solvent and the role of the $\pi\sigma^*$ state were addressed as well. Because in this case conical intersections need not be considered and a multitude of excited states had to be computed which would increase the effort of MR calculations significantly, we decided to use for that purpose a more straightforward approach, the aforementioned ADC(2) method in combination with the recently developed methods for excited-state solvation within COSMO.[39,52,53]

COMPUTATIONAL DETAILS

The geometry optimization of DMABN in the ground state was performed at second order Møller−Plesset perturbation theory (MP2)[54] using the split valence polarization basis (SVP).[55] C_{2v} symmetry was used with C_2 along the z axis and the benzene ring located in the yz plane. The calculations on electronically excited states were performed using the complete active space self-consistent field (CASSCF) method and multireference configuration interaction with single excitations (MR-CIS) and with single and double excitations (MR-CISD), accounting for dynamic electron correlation effects. The active space chosen for the CASSCF wave functions was a CAS(10,9) consisting of 10 electrons in 9 active π and π^* orbitals. The active space comprises the π bonding and antibonding orbitals of the benzonitrile and of the amino N atom. In the CASSCF calculations, a state-averaging (SA) procedure was adopted with

equal weights for the lowest three singlet states (SA-3). Based on the molecular orbitals computed at the SA-3-CASSCF(10,9) level, MRCI calculations were performed with an MR-CIS reference space composed of 10 electrons in 9 orbitals (MR-CIS(10,9)), of 8 electrons in 7 orbitals (MR-CIS(8,7)), and with a MR-CISD reference space composed of 6 electrons in 5 orbitals (MR-CISD(6,5). In all cases, the 11 1s orbitals on the carbon and nitrogen atoms were kept frozen. The orbital occupation scheme of the different reference wave functions are collected in Table S1 of the Supporting Information. Size-extensivity corrections were taken into account in single-point calculations according to Pople et al., indicated by (+P).[56]

Atomic natural orbital (ANO)[57] basis sets were used. Geometry optimizations and the determination of the minima on the crossing seam (MXS) have been performed with the (10s6p3d)/[3s2p1d] basis for N and C and (7s)/[2s] for H. The extended basis [4s3p2d] for N and C atoms was also applied in selected cases. The first basis set is termed ANO-DZ, and the second one ANO-TZ. Dipole moments and population analysis data were computed at the MR-CIS level for gas phase and solution.

Three states are included in the state-averaging procedure (SA-3): the ground state and the two low-lying singlet excited states LE and CT. The twisting (θ) and wagging (δ) angles of the amino group of DMABN were chosen as reaction coordinates to construct energy curves and energy surfaces for the S_1 and S_2 states. The twisting coordinate was defined as $\theta = (\tau_1 + \tau_2)/2$, and the wagging coordinate as $\delta = (\tau_1 - \tau_2)/2$, where τ_1 and τ_2 are the torsional angles $C_2C_1N_1C_6$ and $C_2'C_1N_1C_6'$, respectively (Figure 1). MRCI and ADC(2) calculations were performed for gas phase and AN solution. Solvent effects were taken into account in single-point calculations by means of the conductor-like screening model.[52,53] Nonequilibrium and equilibrium versions were used for the excited states in solution for MRCI as described in refs 58 and 59. For a discussion concerning the excited-state ADC(2)-COSMO calculations, see ref 39. COSMO parameters are given in the Supporting Information. Franck−Condon excitations and fluorescent transitions were treated at the nonequilibrium level, whereas for the reaction paths the

Table 1. Computed Vertical Excitation Energies, ΔE (eV), of the Two Lowest Singlet Exited States of DMABN at the MP2/SVP Optimized Ground-State Geometry in C_{2v} Symmetry (θ, δ = 0°)

method	state	DZ	+P/DZ	TZ	+P/TZ
SA3-CASSCF(10,9)	$^1B_2$ (LE)	4.626 (0.008)[a]	–	4.632	–
	$^1A_1$ (CT)	5.969 (0.667)	–	5.929	–
MRCIS(10,9)	$^1B_2$ (LE)	4.621 (0.026)	4.516	4.598	4.468
	$^1A_1$ (CT)	4.984 (0.670)	4.662	4.936	4.601
MRCIS(8,7)	$^1B_2$ (LE)	4.705 (0.025)	4.325[b]	4.768	4.433
	$^1A_1$ (CT)	5.269 (0.688)	4.902[c]	5.113	4.738
MRCISD(8,7)	$^1B_2$ (LE)	5.054	4.438	5.061	4.470
	$^1A_1$ (CT)	5.606	4.917	5.599	4.941
MRCISD(6,5)	$^1B_2$ (LE)	5.361	4.525	5.382	4.617
	$^1A_1$ (CT)	5.736	5.100	5.727	5.124
CASPT2/ANO[d] (C_2) (CASSCF (10,9)/ANO geom.)	^1B (LE)	4.05 (0.010)			
	^1A (CT)	4.41 (0.416)			
CASPT2[e] (CASSCF (12,11)/6-31G(d) geom.)	LE	4.297			
	CT	4.610			
CC2/TZVPP[f]	LE	4.41			
	CT	4.77			
exptl[g]	S_1^0 (LE)[h]	3.995			
	S_1 (LE)[i]	4.130			
	S_2 (CT)[i]	4.569			

[a]Oscillator strengths (absorption) are given in parentheses. [b]Total energy of $^1B_2$(LE) state: −455.6544360 au, calculated with the ANO-DZ basis set (atomic natural orbital (ANO) basis set - (10s6p3d)/[3s2p1d] basis for N and C and (7s)/[2s] for H) and Pople correction (+P) . [c]Total energy of $^1A_1$(CT) state: −455.6332238 au calculated with the ANO-DZ basis set and Pople correction (+P). [d]Ref 23. [e]Ref 30. [f]Ref 31. [g]Refs 43 and 45. [h]0−0 transition. [i]Band maximum.

equilibrium approach was used. In the latter case full equilibrium conditions are assumed for the excited states.

Geometries of LE and CT stationary points, and the MXS between those two states were optimized at the MR-CIS level using analytic MR-CI gradients[60,61] and nonadiabatic coupling vectors.[62,63] MR-CIS second derivatives of the energy were computed numerically using analytically calculated first derivatives. The MP2 and ADC(2) calculations have been performed using the Turbomole program.[64] Details on the energy convergence parameters can be found in the Supporting Information. All other calculations have been carried out with the program system COLUMBUS[65,66] using its parallel version.[67,68]

■ RESULTS AND DISCUSSION

Vertical Excitation of DMABN. To assess the accuracy of the different multireference approaches used, the two low-lying vertical excitation energies of DMABN were computed at CASSCF, MRCIS, and MRCISD levels of theory using the ANO-DZ and ANO-TZ basis sets and compared to the experimental gas phase data (Table 1). It should be noted that the absorption maximum $\nu^{max}(S_2,abs)$ in the gas phase comes directly from the experimental spectrum, whereas the $\nu^{max}(S_1,abs)$ is hidden under the strong S_2 absorption and its value was obtained after extrapolation.[43] The (10,9), (8,7), and (6,5) reference spaces were tested in MR-CIS and MR-CISD calculations.

At all computational levels, the transition to the $S_1(^1B_2)$ state possesses a small oscillator strength. It involves mainly a HOMO(N_{amino},N_{cyano},C_{ph})−LUMO+1(C_{ph}) transition with dominant local excitation character. The $S_2(^1A_1)$ state shows a strong intensity. It is due to a HOMO(N_{amino},N_{cyano},C_{ph})− LUMO(N_{cyano},C_{ph},N_{amino}) transition which possesses partial charge-transfer character. The orbitals involved in the

transitions above are plotted in Figure S1a of the Supporting Information. The CASSCF calculation overestimates the energy of the $S_2(^1A_1)$ state by 1.4 eV as compared to the experimental value, similar to the results reported in refs 8 and 28. The energetics is significantly improved at the MRCI level. The single excitation correction produces an energy decrease of $S_2(^1A_1)$ by ∼1 eV, whereas the energy of the $S_1(^1B_2)$ state is not changed. Reducing the reference CAS from (10,9) to (8,7) leads to an increase of the $S_1(^1B_2)$ and $S_2(^1A_1)$ energies by 0.1− 0.3 eV. The single and double excitations calculations (MR-CISD(6,5)+P and MR-CISD(8,7)+P) do not improve the excitation energies and even lead to their slight increase. The extended basis set, ANO-TZ, changes the energies of both excited states only slightly. Higher-order excitations using the Pople correction lower the absorption energies significantly, bringing them into quite good agreement with experimental values. The calculated $\Delta(S_1/S_2)$ gaps computed at the MRCIS(8,7)+P and MRCISD(6,5)+P levels agree well with the experimental data (Table 1). Among the methods tested, the MRCIS(8,7)+P/ANO-DZ provides the best approach with respect to experimental S_1 and S_2 vertical excitation energies (both excited states are overestimated by about 0.3 eV) and reproduces the $\Delta(S_1/S_2)$ gap of 0.57 eV very well. In view of the good performance of the MRCIS(8,7)+P/ANO-DZ level and because of considerations of computational efficiency, all calculated transition energies presented below were performed with this approach.

Optimization of the S_0, LE, and CT structures. Next, the optimized geometries in the Franck−Condon (FC) region are discussed (Figure 1a−c). The optimized geometries of S_2/S_1 MXS state and the $\pi\sigma^*$ state, discussed in the following sections, are given in Figure 1d,e. The MP2/SVP calculations for the S_0 geometry yield a minimum at C_s symmetry (i.e., θ = 0.0°) and a wagging angle of δ = 10.2°. The experimental θ and

δ angles obtained from X-ray diffraction measurements (at 253 K) are 0.0° and 7.7°, respectively.[69] Microwave spectroscopic measurements in the gas phase lead to a δ angle of about 15°.[70] The MP2 calculations reproduce well the amino C_1-N_1 and C_4-C_5 bond lengths ($\Delta = 0.005-0.007$ Å), whereas the calculated phenyl C–C and cyano C_5-N_2 bond lengths are longer by ~0.02–0.03 Å as compared to the crystallographic data. The C_{2v} symmetry structure ($\theta = \delta = 0°$) is only slightly higher in energy by 0.06 kcal/mol than the C_s structure. The bond lengths of C_s and C_{2v} optimized structures are very similar. The ground-state DMABN structure was also calculated with the MRCIS(8,7) method (Figure 1a); the bond distances are comparable with the MP2 bond distances (Δ up to 0.007 Å). It should be noted that the MRCIS(8,7) method reproduces better the cyano C_5-N_2 bond length (1.157 Å versus 1.145 Å exptl), whereas with MP2/SVP and CC2/TZVPP[27] it is too large by 0.035 Å. The phenyl moiety shows a quinoidal distortion along the long molecular axis (i.e., shortened C_2-C_3, $C_{2'}-C_{3'}$ bond lengths). The $C-N_{amino}$ bond distance (calcd, 1.372 Å (MP2); exptl, 1.365 Å) is shorter than a normal single C–N bond (~1.46 Å)[71] because of the resonance between the dimethylamino part and the adjacent benzene ring.

Around the Franck–Condon region, the S_1 state is assigned to the LE state. The LE geometry was optimized without symmetry constraint at the MRCIS(8,7)/ANO-DZ level. The optimized LE geometry reveals a twisting angle θ of 13.9°, a wagging angle δ of 0°, and out-of-plane benzene H atoms (dihedral HCCH angle, −5°) (Figure 1b). The calculated θ and δ values can be compared to the experimental ones of $\theta = 30°$; $\delta = 0°$ obtained by microwave spectroscopy;[70] $\theta = 30°$ by time-of-flight mass spectrometry;[72] $\theta = 26°$ by resonant enhanced two-photon ionization;[73] and $\theta = 25°$, $\delta = 3°$ by rotationally resolved fluorescence spectra.[74] It should be noted that the potential energy curve of the LE state with regard to the twisting coordinate appears quite shallow in the region of 0–30° (see below), allowing the twisting angle to vary largely. The LE geometry is characterized by an elongation of the phenyl C_1-C_2 and C_2-C_3 bond lengths by 0.017 and 0.036 Å, respectively, and by slight variations of the C_5-N_2, C_2-N_1, and C_4-C_5 bond lengths (up to 0.008 Å) as compared to the ground state. The CC2/TZVPP calculations of DMABN (C_2) show similar θ and δ values of 19° and 0°, respectively, and similar trends in bond length changes.[26] The intense ultraviolet (UV) absorption due to the S_2 state is assigned to the CT state with a large dipole moment in the FC region. In the FC region, the S_2(CT) geometry is not stable. Instead, the CT state twists around the C_1-N_1 bond and shows a minimum (then in the S_1 state) at a twisting angle of 90.2° and a wagging angle of 0.8°. Selected structural data are given in Figure 1c. The small deviations from 90° and 0° are not considered to be significant and are due to the shallow energy surface in this region of angles. The optimized CT geometry is characterized by significant quinoidal distortions (i.e., shortened C_2-C_3 and $C_{2'}-C_{3'}$ bond lengths) as compared to the ground state and also to the LE structure. The most significant geometrical change was found for the C_1-N_{1amino} bond, which elongates by 0.06 Å, facilitating rotation around C–N bond. The C_4-C_5 bond is shortened by ~0.02 Å, whereas the C≡N bond is slightly stretched by 0.01 Å as compared to the S_0 geometry. Bond length changes have been estimated experimentally by comparing the vibrational frequencies in the CT state to those in the ground state. Numerous efforts were made to measure

the vibrational frequencies of DMABN in the CT state by picosecond IR,[15,16] picosecond time-resolved resonance Raman spectroscopies[46] and femtosecond stimulated Raman spectra.[75] The elongation of the $C-N_{amino}$ and $C-N_{cyano}$ bonds in the CT state was confirmed by these experimental studies, supporting the TICT structure in which the π-conjugation including the $C-N_{amino}$ bond is broken. For comparison, the CT geometry obtained by CC2/TZVP calculations[27] showed a saddle point structure with a twisting angle at 90°, a wagging angle of 0°, and an out-of-plane angle at 41°. The bond length changes (S_0 to CT) calculated by CC2 and MRCIS(8,7) methods follow the same trend.

Absorption and Emission Energies in Gas Phase and Acetonitrile. The calculated vertical excitation energies, minimum-to-minimum and vertical fluorescence energies in the gas phase and in AN solution are presented in Table 2.

Table 2. MRCIS(8,7)+P/ANO-DZ Vertical (vert) Absorption and Fluorescence (fl) Energies (eV) and Minimum-to-Minimum (m-m) Energies in the Gas Phase and in AN Solution of Optimized Ground-State, LE, and CT structures of DMABN

structure (symmetry)	state	gas phase		AN	
		calcd[a]	exptl[b]	calcd[noneq]	exptl[c]
gr. state (C_{2v})	vert. 1^1B_2 ($\pi\pi*$)	4.32 (0.025)	4.13	4.34	3.86
	vert. 2^1A_1 ($\pi\pi*$)	4.90 (0.688)	4.57	4.75	4.24
LE state (C_2)	T_e^d 1^1B ($\pi\pi*$)	4.13		4.15	
	ν_{00} 1^1B ($\pi\pi*$)	(3.95)[e]	3.998[f]		
	fl 1^1B ($\pi\pi*$)	3.93 (0.012)	3.68	3.94	3.44
CT state (C_1)	T_e^d 2^1A ($\pi\pi*$)	4.29		3.90	
	fl 2^1A ($\pi\pi*$)	3.27 (0.004)	3.55 (extrap.)	2.77	2.52

[a]Oscillator strengths (absorption) are given in parentheses. [b]Ref 43. [c]Refs 3, 21, and 49. [d]Adiabatic excitation energy (rel to the ground-state minimum). [e]Position of 0–0 transition (approximation); the result in ref 27 was used. ν_{00} energy is about 0.2 eV below T_e energy for LE state. [f]Laser-induced fluorescence (LIF) excitation spectrum in the gas phase, ref 45.

The calculated oscillator strength for the vertical excitation to the S_2(CT) state is large and will dominate the absorption intensity in comparison to the S_1(LE) state. Going from gas phase to AN solution the experimental absorption energy decreases from 4.57 to 4.24 eV,[3,21,49] resulting in a decrease of the $\Delta E(S_1S_2)$ energy gap from 0.44 eV (gas) to ~0.38 eV (AN). In accordance with the experiment, the calculations in AN solution showed a decrease of the vertical excitation energy of the S_2 state (4.90 eV (gas) to 4.75 eV (AN)) and of the $\Delta E(S_1,S_2)$ energy gap from 0.58 eV (gas) to 0.41 eV (AN) (Table 2). A similar trend of the solvent effects (aprotic and protic solvent) was predicted from the average solvent electrostatic potential from molecular dynamics (ASEP/MD) calculations of the DMABN UV/vis spectra.[76]

The energy diagrams of the LE → TICT process for DMABN in the gas phase and AN solution are compared in Figure 2.
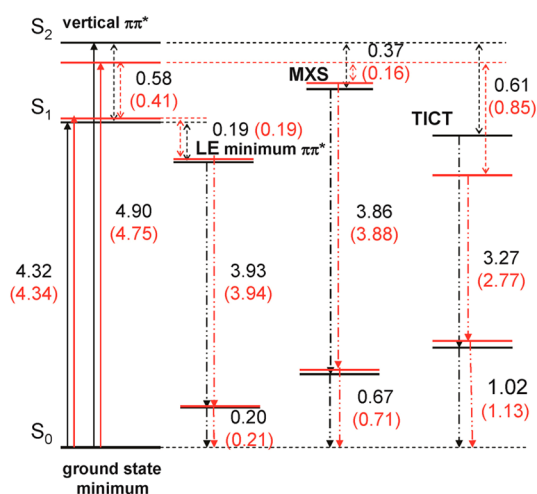
Figure 2. LE/CT energy diagram (eV) of DMABN in vacuum (black) and acetonitrile (red) calculated at the MRCIS(8,7)+P/ANO-DZ level. The transition energies in acetonitrile solution are given in parentheses.

The calculated ΔE for the LE → TICT reaction in the gas phase is positive (0.16 eV) in keeping with the positive formation enthalpy (0.05 eV), determined by extrapolation from plots of ΔH vs the solvent polarity parameter.[43] In line with the experiment, CASPT2 calculations have predicted a positive ΔE of 0.41 kcal/mol (0.02 eV) for a twisted ICT and of 7.10 kcal/mol (0.31 eV) for a planar ICT.[30] The experimental and calculated endothermic reaction LE → ICT of DMABN in the gas phase is in line with the absence of dual fluorescence in the gas phase. The CC2/SVP[31] calculations, however, have predicted a small exothermic gas-phase LE → ICT reaction of DMABN ($\Delta E = -1.84$ kcal/mol/-0.08 eV). This result was corrected by using higher-order coupled cluster single and double excitations with noniterative triple-corrected excitation energy (CCSDR(3)) calculations, which shifted the ICT level to higher energy by ~0.2 eV relative to the LE level.[27]

In AN solution, the ΔE for the reaction LE → ICT calculated at the MRCIS(8,7)+P/ANO-DZ level is negative (-0.25 eV), which is consistent with the experimental exothermic reaction ($\Delta E = -0.28$ eV).[49] The exothermic LE → ICT reaction is in accordance with the ICT producing dual fluorescence in AN solution.

Finally, DMABN relaxes into S_0 via fluorescence emission from S_1. The emission energy at the LE geometry is 3.93 eV in the gas phase and 3.94 eV in AN. The experiment predicts a somewhat larger solvent effect on LE emission energies: 3.68 eV in the gas phase[43] and 3.44 eV in AN.[21] The AN solvent stabilizes the CT structure significantly more than the LE structure leading to a negative energy of the LE → CT reaction (Figure 2). The calculated emission energy of 3.27 eV for the optimized TICT structure in the gas phase shows good agreement with the experimental ICT emission energy of 3.55 eV for DMABN in the gas phase (extrapolated from solvent series).[43] Both experimental and calculated ICT emission transitions of DMABN in AN are found at lower energies, 2.52[49] and 2.77 eV, respectively. The AN solvent produces greater stabilization of the ICT structure and hence a red-shift of the emission maximum for DMABN in the TICT state. Similar results were obtained recently from ADC(2)/COSMO calculations[39] and from ASEP/MD calculations.[76]

In Table 3, the MRCIS(8,7)/ANO-DZ dipole moments of the GS, LE, and CT states are compared to the experimental

Table 3. Calculated Dipole Moments, μ (Debye), for DMABN in Comparison with Experimental Data

method	μ (GS in C_{2v})	μ (LE)	μ (CT)
MRCIS(8,7)/ANO-DZ	7.1	9.6	15.3
CC2[a]	7.4	10.1	13.3
CASSCF(12,11)[b]	6.1	6.0/6.6[c]	13.5
exptl[d]	6.6	9.7/9	17 ± 1

[a]Ref 31. [b]Ref 29. [c]Ref 28. [d]Refs 77 and 78.

values[77,78] and to those obtained in other calculations. The computed dipole moments are in good agreement with the corresponding experimental data.

Torsional Energy Curves and Two-Dimensional Energy Surfaces of DMABN in Gas Phase and Acetonitrile. The MP2/SVP optimized ground-state geometry of DMABN in C_{2v} symmetry ($\theta, \delta = 0°$) was taken as starting point for computing potential energy curves along the twisting angle (rotation around the C_1-N_1 bond; $\theta = 0, 15, 30, 45, 48, 49, 50, 60, 75, 90°$) and the two-dimensional potential energy surfaces in both the twisting and wagging ($\delta = 0, 5, 10, 15, 20°$) coordinates in the gas phase and AN solution. The shape of the most important MOs can be found in Figures S1a,b and S2a,b of the Supporting Information.

Inspection of the potential energy curve along the twisting path (Figure 3a) shows the two minima in the S_1 state: the LE state at the nontwisted geometry ($\theta = 0°$) and the CT state at the perpendicular twisted geometry ($\theta = 90°$) of DMABN. The energy of the nontwisted geometry is lower by 0.27 eV as compared to S_1 at twisted DMABN.

As shown in Figure 3a, with the increase of the twisting angle, the S_1 and S_2 states cross at ~50°. Inspecting the calculated fragment charge of the phenyl ring plus CN group, $q_{ring+CN}$, computed from a Mulliken population analysis,[79] illustrates charge transfer in the S_2 state that is only slightly larger than that in the S_1 state for the nontwisted form (Figure 3b). Along the twisting coordinate between 0° and 48°, the charge-transfer character of the S_2(CT) state progressively increases by ~0.1 e: the charge $q_{ring+CN}$ decreases from -0.3 e to -0.4 e (the main contribution belongs to the acceptor (A) phenyl charge), whereas concomitantly the charge of the donor (D) amino group increases from $+0.3$ e to $+0.4$ e. At a twisting angle of ~50°, the character between the two states is abruptly exchanged because of the intersection of the two states. After the intersection the state characters are CT for S_1 and LE for S_2. Along the twisting coordinate from 50° to 90°, the energy of the S_1(CT) state decreases with the increase of its charge transfer (Figure 3). The large dipole moment and large charge separation make the CT excited state strongly sensitive to the solvent polarity. Figure 4 displays the S_1 and S_2 energy surfaces in the torsion and wagging coordinates. It can be seen that altering the wagging angle does not lift this degeneracy significantly.

The calculated potential energy curves, the fragment charge $q_{ring+CN}$, and energy surfaces of DMABN in AN (equilibrium solvation conditions) are plotted in Figures 5a,b and 6, respectively. For comparison, the nonequilibrium solvent calculations of the potential energy curves and surfaces of DMABN were also calculated. They are presented in the Supporting Information (Figure S3 and Figure S4). The
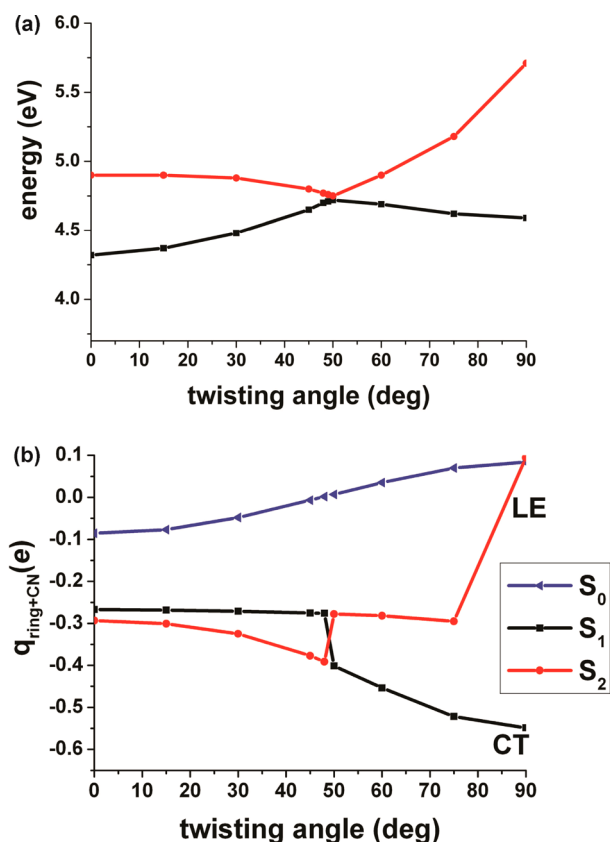
Figure 3. Rigid potential energy curves along the twisting angle θ (the wagging angle δ is fixed at 0°) (a) and charge transfer, $q_{ring+CN}$ (e) (b) for the two lowest singlet excited states of DMABN in the gas phase at the MRCIS(8,7)+P/ANO-DZ level. Energies are given relative to the S_0 energy of the ground-state minimum at C_{2v} symmetry (θ, δ = 0°).
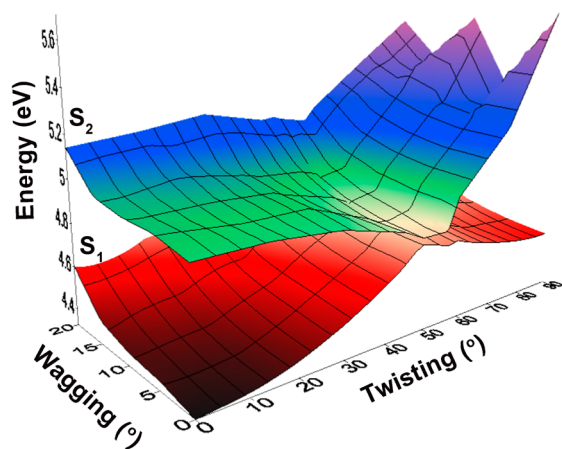

Figure 5. Potential energy curves along the twisting angle θ (the wagging angle δ is fixed at 0°) (a) and charge transfer, $q_{ring+CN}$ (e) (b), of the two lowest singlet excited states of DMABN in acetonitrile for equilibrium solvent conditions at the MRCIS(8,7)+P/ANO-DZ level.

Figure 4. Potential energy surfaces along the twisting (θ) and wagging (δ) coordinates of the two lowest singlet excited states of DMABN in the gas phase at the MRCIS(8,7)+P/ANO-DZ level.

Figure 6. Potential energy surfaces along the twisting (θ) and wagging (δ) coordinates of the two lowest singlet excited states of DMABN in acetonitrile for equilibrium conditions at the MRCIS(8,7)+P/ANO-DZ level.

computed potential energy curves and surfaces are very similar in both solvation cases.

In AN, the S_1 and S_2 energy curves resemble those in the gas phase up to $\theta = 50°$, only the energy gap, $\Delta(S_1/S_2)$, is smaller for AN solvation. The S_1 energy curve in AN shows also two minima as in the gas phase, but unlike the gas-phase curves the lower energy minimum appears at the twisted (90°) DMABN form (by −0.46 eV). There is a quite strong stabilization of the
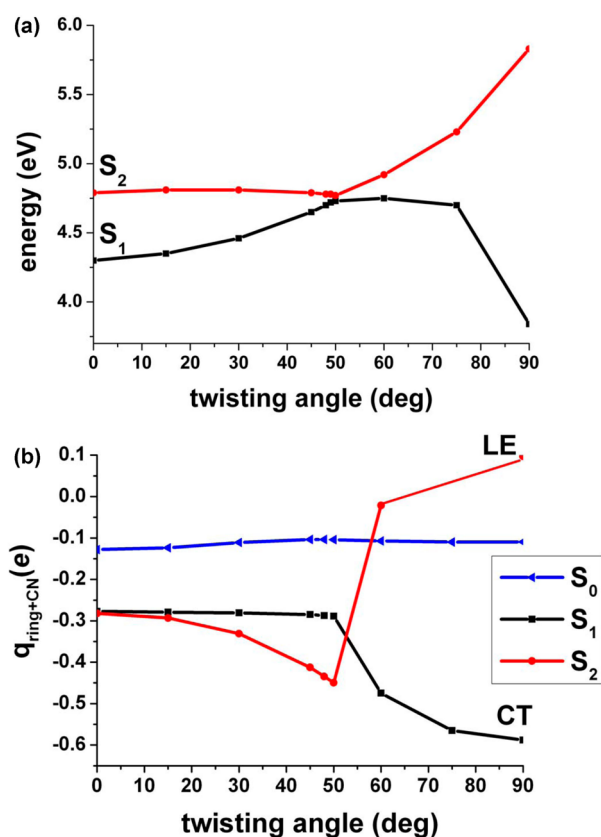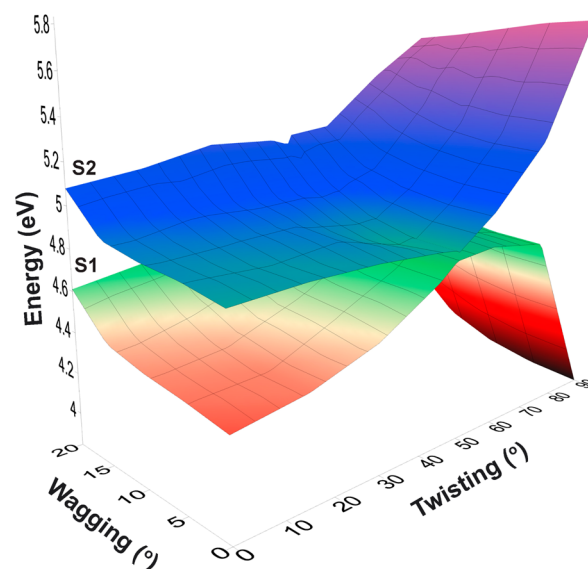
S_1 (CT) state at $\theta = 90°$, but the gap to the S_0 state remains still quite large (∼2.9 eV).

To illustrate the stabilization of the TICT state in solution, the fragment charge $q_{ring+CN}$ for S_0, S_1, and S_2 state were calculated in AN (equilibrium condition) (Figure 5b).

Inspection of the charge transfer in the S_1 and S_2 states for the gas phase (Figure 3b) and solution (Figure 5b) for the nontwisted DMABN form shows a slight solvent effect on the charge separation. The small difference in charge transfer for the S_1 and S_2 states found in the gas phase disappears in solution. On the other hand, the solvent causes a somewhat larger charge separation (0.09 e (gas), 0.13 e (AN)) in the nontwisted ground-state form. Its value remains almost constant after twisting. Along the twisting coordinates between 0° and 55°, the charge transfer of the S_2(CT) state progressively increases, following the trend found in the gas phase. The calculations predict a somewhat larger charge separation in solution for the S_2(CT) state (increases by ~0.2 e. from 0° to ~50° twisting); the charge of the donor (D) amino group increases within the above-mentioned torsion range from +0.3 e to +0.5 e (and the $q_{ring+CN}$ charge decreases from −0.3 e to −0.5 e accordingly, Figure 5b), whereas in the gas phase, q_{amino} and $q_{ring+CN}$ charges are changed by only 0.1 e within that range of the twist angle. It should be noted that the charge transfer gets larger in solution (compared to the gas phase) primarily at twisting above 30°. The fragment charge of the S_1(LE) state is hardly increased (up to 0.05 e) by the solvent effect in the twisting range of 0° to ~50°.

At a twisting angle of ~50°, the character between the two states is exchanged (Figure 5a) in analogy to the situation described for the gas phase. The fragment charge separation for the twisted (90°) DMABN structure in solution remains larger by ~0.1 e (going from 0° to 90° twist angle, $q_{ring+CN}$ decreases by 0.31 e (AN) versus 0.25 e (gas)). After the intersection, the S_2 state obtains LE character and its charge separation abruptly tends to zero and the S_2(LE) state loses practically any charge-transfer character. In the gas phase this charge transfer changes more gradually. The larger charge separation of the S_1(CT) state in solution as compared to that in the gas phase agrees with its larger stabilization in polar solvent and with the fact that the minimum of the S_1(TICT) state is lower in energy than that of the S_1(LE) state.

In AN solution, the S_1 and S_2 energy curves intersect at approximately the same twisting angle of ~50° as in the gas phase; therefore, the S_2/S_1-MXS appears to be quite independent of the environment polarity. A survey of the S_1 and S_2 energy surfaces of DMABN in the gas phase and AN (Figures 4 and 6) shows that the wagging coordinate does not strongly affect the $\Delta E(S_1 S_2)$ energy difference in the S_1/S_2 crossing region and could play only a small role in assisting the twisting intracharge transfer mechanism.

In Figure 7, the energy gradient difference vector **g** and the nonadiabatic coupling vector **h** characterizing the branching space of the intersection cone[63,80−82] are displayed for the MXS structure between S_2 and S_1 (Figure 1d). These two vectors describe bond-stretch motions within the benzene ring and with the two substituents but do not contain the twisting angle θ. Thus, in agreement with the calculations of Gómez et al.[29] and Kochman et al.[42] we find that this coordinate is not part of the branching space and thus will not participate in the nonadiabatic transfer from S_2 to S_1. The **g**-vector shows modes along the quinoidal C_2/C_3 and $C_{2'}/C_{3'}$ coordinates as suggested in ref 27.

The Role of the $\pi\sigma^*$ State. As already discussed in the Introduction, an alternative deactivation path via a rehybridized ICT (RICT) in a bent $\pi\sigma^*_{CN}$ state was suggested a long time ago[8,9] and has been taken up recently emphasizing the importance of this state for the deactivation processes in
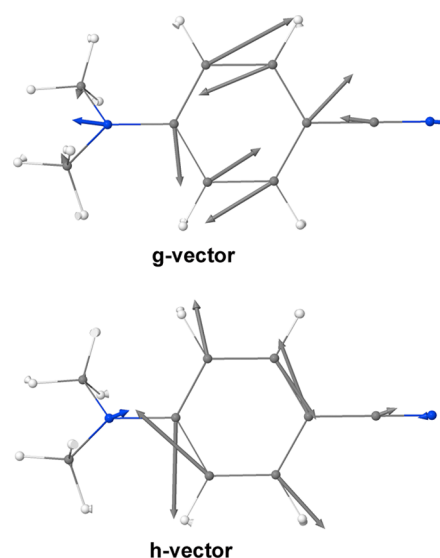

g-vector

h-vector

Figure 7. **g**- and **h**-vectors for the MXS between S_2 and S_1 computed at the MRCIS(8,7)/ANO-DZ level in the gas phase.

DMABN (see ref 38 and references therein). To compare with the twisting pathway described in the previous section, ADC(2) calculations have been performed along the $C_4C_5N_2$ angle (see Figure 1) similar to the investigations reported in ref 36.

Figure 8a shows the potential curves under C_s symmetry restriction for several excited states in the gas phase in dependence of the CCN angle. Most of the curves increase in energy when starting at the linear geometry at 180°, only the $\pi\sigma^*$ is stabilized, similar to the findings in refs 8 and 36. In spite of the significant stabilization of this state, it still is located ~1 eV above the LE minimum (Table 4). This fact led to the conclusion that at least in the gas phase this state would not contribute significantly to the deactivation dynamics in DMABN.[10] Moreover, analysis of the Hessian matrix showed several imaginary frequencies related to out-of-plane modes. Starting a geometry optimization from a slightly out-of-plane distorted geometry led to the LE minimum structure. Thus, at least in the gas phase the $\pi\sigma^*$ state does not correspond to a stable structure at the ADC(2) level. In AN solution (Figure 8b), because of the large dipole moment of the $\pi\sigma^*$ state (15.9 D), polar solvation stabilizes this state significantly with respect to the two lowest $\pi\pi^*$ states. Table 4 shows that at the energy minimum (in the one-dimensional potential energy curve) the $\pi\sigma^*$ state is even a little lower than the LE state. Thus, the $\pi\sigma^*$ state is energetically accessible in comparison to the absorption energy of the bright S_2 state (Table 1). However, the Franck−Condon factors for the transition between the ground and $\pi\sigma^*$ states will certainly not favor this transition because of the strong bending of the CCN group in the latter state in comparison to the linear arrangement in the ground state.

The Photodynamical Deactivation Model. The discussion of the photodynamical deactivation model orients itself on the following observations reported in this work. A minimum on the crossing seam between the LE and CT states (S_1/S_2) has been located at MRCIS level as a twisted structure (Figure 1d) as postulated in the TICT model. In agreement with the results obtained from CASSCF calculations by Gómez et al. and Kochman et al.,[29,42] it is found that the twisting motion is not included in the branching space but characterizes the intersection seam. As a consequence, the seam will be accessible via a wider range of twisting angles. There is a
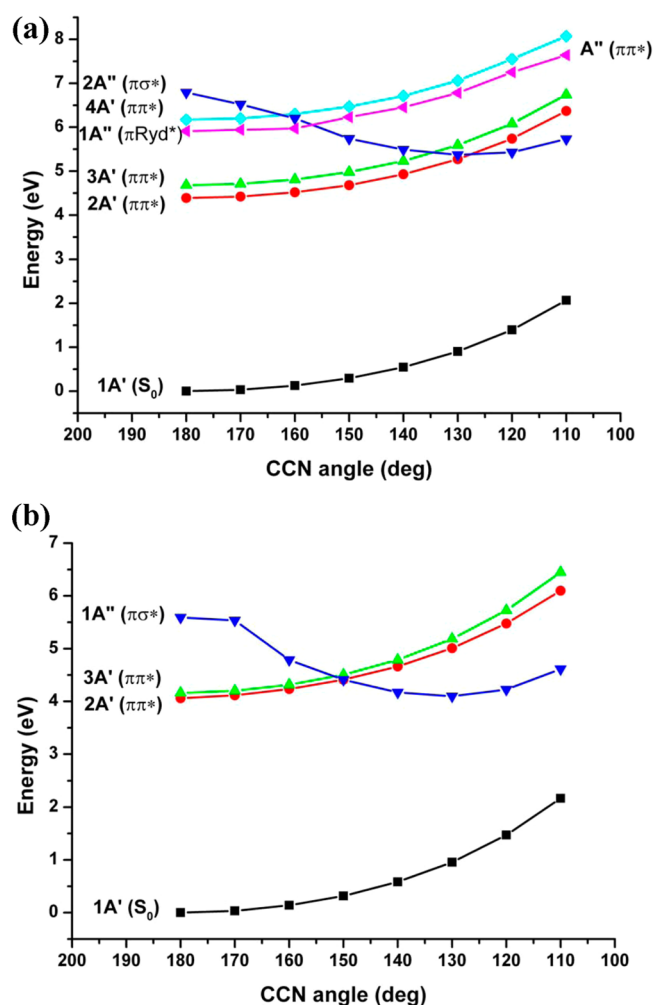
Figure 8. Rigid potential energy curves along the CCN angle for the lowest singlet excited states of DMABN under C_s symmetry restriction (a) in the gas phase and (b) in AN solution at the ADC(2)/TZVP level. Starting point is the MP2/SVP optimized ground-state geometry of DMABN (C_{2v}, ∠CCN = 180°).

Table 4. Energies, ΔE (eV), Relative to the Ground-State (C_{2v}); Oscillator Strengths, f; and Dipole Moment, μ (Debye), for the Low-Lying Excited States in DMABN Using the ADC(2)/TZVP Method

	in vacuo			AN sol		
structure[a]/state	ΔE	μ	f	ΔE	μ	f
gr. state/S_1	4.39	11.2	0.036	4.23	13.0	0.041
gr. state/S_2	4.68	14.8	0.597	4.20	17.6	0.675
LE (min.)/S_1	m-m 4.18	11.8	0.036	3.89	13.6	0.040
$\pi\sigma$*/S_1	5.10	18.7	0.000	3.85	15.9	0.000
MXS/S_1	4.21	16.4	0.219	3.48	18.5	0.244
TICT/S_1	3.99	17.9	0.000	3.17	19.6	0.000

[a]Optimized geometries of LE, MXS, TICT structures at MRCIS (8,7)/ANO-DZ level and of $\pi\sigma$* structure at ADC(2)/TZVP level were used.

barrierless reaction path starting at the Franck–Condon point in S_2 to the twisted CT minimum on the S_1 surface (rigid torsion, Figure 3, gas phase). Two minima have been located on the S_1 surface, a quasi-planar LE structure and an orthogonal CT structure (panels b and c of Figure 1, respectively). The $\pi\sigma$* state is energetically too high to play a significant role in

the gas phase dynamics. Starting from the bright S_2 state, the photodynamics will be driven by the twisting around the CN bond between the phenyl ring and the dimethylamino group because of the energetic stabilization of that state. However, the nonadiabatic transition to the S_1 state is determined by planar intraring coordinates and not by the torsion. In fact, the recent surface hopping study by Kochman et al.[42] has shown that such a decay should occur at very early stages of the photodynamics, a fact which is also supported by the characterization of the branching space of the conical intersection between S_2/S_1 computed at the MRCIS level. The equilibration between the LE and TICT states will occur on the S_1 surface.

In polar (acetonitrile) solution, the shape of the twisting potential curves is the same as in the gas phase (rigid torsion, Figure 5). The descent from the S_2 Franck–Condon point to the MXS is slightly flatter as compared to the gas phase; only the path from the MXS to the TICT minimum is steeper. Because the evolution of the charge transfer, $q_{\text{ring+CN}}$, in the gas phase and in AN solution is quite similar for torsion angles up to the intersection, it is expected that the qualitative character of the branching space will not change and that also in solution it will be determined by intraring vibrations and not by the torsional motion. Thus, it is quite likely that also in polar solution the initial dynamics will primarily proceed as in the gas phase and that the major fraction of the nonadiabatic decay will lead to the LE state from which equilibration with the TICT will occur. Because of the enhanced stability of the latter state in polar solution as compared to the gas phase case, the TICT state will be predominantly populated.

The strong stabilization of the $\pi\sigma$* state in AN solution has already been noted (Figure 8), leading to a possible contribution to the photodynamics, as emphasized in refs 11,36−38, and 83. However, starting with the photodynamics in the Franck−Condon point, CCN bending of the nitrile group leads to a destabilization of the S_1 and S_2 $\pi\pi$* states so that at least in the initial phase of the dynamics, population of the $\pi\sigma$* state by this mode cannot be expected. As described in the previous paragraph, similar to the gas phase, the photodynamics will start in the S_2 state with a twisting of the $N(CH_3)_2$ group and a rapid decay to the LE structure. Because of the comparable stability of the LE and $\pi\sigma$* structures in AN, participation of the latter structure in the later phases of the photodynamics is possible. From our static calculations it is difficult to predict to which extent the CCN bending motion will be actually activated. In any case, the final structure (in addition to the LE minimum) in the excited state should be the TICT structure.

In our MRCIS calculations and also in the ADC(2) calculations of Kochman et al.[42] for the gas phase no additional partially twisted (pTICT) minimum was found in contrast to the CASSCF optimizations performed by Coto et al.[38] In fact, the twisting angle of −53.4° reported in this latter work coincides almost exactly with the twisting found for the MXS (Figure 1d), and Figure 5 shows a barrierless reaction path on S_1 to the TICT structure. Thus, a pTICT structure stable over the time of several nanoseconds, as required by the proposal suggested in ref 38 (that this structure is the source of fluorescence), does not seem likely according to our findings.

■ CONCLUSIONS

The mechanism leading to dual fluorescence of DMABN in the gas phase and in acetonitrile solution has been addressed using two computational methods: (i) the multireference config-

uration interaction with single excitations (MRCIS) and (ii) the second-order algebraic diagrammatic construction (ADC(2)) method. Solvent effects have been based on the conductor-like screening model in both approaches.

The MRCIS calculations show that the main absorption proceeds to the S_2 state possessing a charge-transfer (CT) character somewhat larger than that of the S_1 state. In the gas phase as well as in AN solution the excited $S_2(CT)$ state structure facilitates the twisting of the dimethylamino group. Along the twisting coordinate the S_2 state is stabilized, crossing the S_1 state at ∼50° in the minimum on the crossing seam (MXS). It is important to note that in agreement with the findings of Gómez et al.[29] the twisting angle is not part of the intersection space, which makes the intersection seam accessible for a larger range of twisting angles. This result is also well in line with the results of recent nonadiabatic dynamics simulations[42] which show a very fast deactivation from S_2 to S_1 within 8.5 fs at practically planar geometries. The calculated fragment charge $q_{ring+CN}$ in the gas phase and in solution are used to describe the character changes of both states at the conical intersection. The position of the conical intersection appeared quite independent of the environment used. The larger charge separation found for the twisted DMABN (TICT) structure explains the enhanced stabilization of the $S_1(TICT)$ state in polar solvent and hence the lower energy minimum of $S_1(CT)$ state in comparison to the $S_1(LE)$ state.

The ADC(2) calculations have been used primarily to investigate the role of the CCN bent $\pi\sigma^*$ state. The results show that for the gas phase this state is energetically too high and should not participate substantially in the photodynamics starting from S_2. In AN solution this state is significantly stabilized and energetically accessible from the Franck–Condon excitation. The initial dynamics starting in the $S_2(\pi\pi^*)$ state will begin with the $(CH_3)_2N$ twisting or, as outlined in ref 27, also by pyramidalization of the carbon ring atom next to the nitrogen. The CCN bending, however, would lead to an initial destabilization of the $\pi\pi^*$ states. Nevertheless, in polar solution, because of the comparable stability of the LE and planar $\pi\sigma^*$ states, the latter state could play a role in a later phase of the dynamics. Finally, DMABN should either arrive in the $S_1(LE)$ or $S_1(TICT)$ structures from which fluorescence can occur. Because of the close structural similarity of the pTICT structure with the MXS structure, the former does not appear to be sufficiently stable to act as the origin of fluorescence with a lifetime of 2.9 ns. Future work is certainly needed to shed more light on the question of whether the two different transient lifetimes found for absorption (4.8 ns) and fluorescence (2.9 ns)[38] really point to the presence of two independent ICT structures or whether an explanation based on one ICT structure can be found.

ASSOCIATED CONTENT

Ⓢ Supporting Information

Details of convergence thresholds and solvent model parameters; definition of the CAS reference spaces; figures of orbitals for the twisting angles 0°, 30°, 60° and 90°; plots potential energy curves and charge transfer along the twisting angle θ; plots of potential energy surfaces along the twisting (θ) and wagging (δ) coordinates for nonequilibrium solvent conditions; Cartesian coordinates of DMABN in ground state, LE, CT, MXS, and $\pi\sigma^*$ states. The Supporting

Information is available free of charge on the ACS Publications website at DOI: 10.1021/acs.jpca.5b03282.

AUTHOR INFORMATION

Corresponding Authors

*E-mail: ivelina@svr.igic.bas.bg.

*E-mail: hans.lischka@univie.ac.at. Phone: +1-806-834-6769.

Notes

The authors declare no competing financial interest.

REFERENCES

(1) Lippert, E.; Lüder, W.; Moll, F.; Nägele, W.; Boos, H.; Prigge, H.; Seibold-Blankenstein, I. Umwandlung von Elektronenanregungsenergie. *Angew. Chem.* **1961**, *73*, 695−706.

(2) Daum, R.; Druzhinin, S.; Ernst, D.; Rupp, L.; Schroeder, J.; Zachariasse, K. A. Fluorescence Excitation Spectra of Jet-Cooled 4-(Diisopropylamino)Benzonitrile and Related Compounds. *Chem. Phys. Lett.* **2001**, *341*, 272−278.

(3) Zachariasse, K. A.; Grobys, M.; Tauer, E. Absence of Dual Fluorescence with 4-(Dimethylamino)Phenylacetylene. A Comparison between Experimental Results and Theoretical Predictions. *Chem. Phys. Lett.* **1997**, *274*, 372−382.

(4) Köhler, G.; Rechthaler, K.; Rotkiewicz, K.; Rettig, W. Formation and Stabilization of Twisted Intramolecular Charge Transfer States in Binary Mixed Solvents. *Chem. Phys.* **1996**, *207*, 85−101.

(5) Rettig, W.; Lutze, S. Mechanistic Considerations for the Dual Fluorescence of Dimethylaminobenzonitrile: A Fluorescence Anisotropy Study. *Chem. Phys. Lett.* **2001**, *341*, 263−271.

(6) Grabowski, Z. R.; Rotkiewicz, K.; Rettig, W. Structural Changes Accompanying Intramolecular Electron Transfer: Focus on Twisted Intramolecular Charge-Transfer States and Structures. *Chem. Rev.* **2003**, *103*, 3899−4031.

(7) Demeter, A.; Druzhinin, S.; George, M.; Haselbach, E.; Roulin, J. L.; Zachariasse, K. A. Dual Fluorescence and Fast Intramolecular Charge Transfer with 4-(Diisopropylamino) Benzonitrile in Alkane Solvents. *Chem. Phys. Lett.* **2000**, *323*, 351−360.

(8) Sobolewski, A. L.; Domcke, W. Charge Transfer in Aminobenzonitriles: Do They Twist? *Chem. Phys. Lett.* **1996**, *250*, 428−436.

(9) Sobolewski, A. L.; Domcke, W. Promotion of Intramolecular Charge Transfer in Dimethylamino Derivatives: Twisting Versus Acceptor-Group Rehybridization. *Chem. Phys. Lett.* **1996**, *259*, 119−127.

(10) Sobolewski, A. L.; Sudholt, W.; Domcke, W. Ab Initio Investigation of Reaction Pathways for Intramolecular Charge Transfer in Dimethylanilino Derivatives. *J. Phys. Chem. A* **1998**, *102*, 2716−2722.

(11) Zgierski, M. Z.; Lim, E. C. The Role of $\pi\sigma^*$ State in Intramolecular Electron-Transfer Dynamics of 4-Dimethylaminobenzonitrile and Related Molecules. *J. Chem. Phys.* **2004**, *121*, 2462−2465.

(12) Lippert, E.; Lüder, W.; Moll, F.; Nägele, W.; Boos, H.; Prigge, H.; Seybold-Blankenstein, I. *Angew. Chem.* **1961**, *73*, 695−706.

(13) Il'ichev, Y. V.; Kühnle, W.; Zachariasse, K. A. Intramolecular Charge Transfer in Dual Fluorescent 4-(Dialkylamino)Benzonitriles. Reaction Efficiency Enhancement by Increasing the Size of the Amino and Benzonitrile Subunits by Alkyl Substituents. *J. Phys. Chem. A* **1998**, *102*, 5670−5680.

(14) Lommatzsch, U.; Brutschy, B. Ab Initio Calculations and Supersonic Jet Studies on the Geometry of 4-Dimethylaminobenzoni-

trile (DMABN) and Related Compounds in the Ground and Excited State. *Chem. Phys.* **1998**, *234*, 35−57.

(15) Okamoto, H.; Inishi, H.; Nakamura, Y.; Kohtani, S.; Nakagaki, R. Picosecond Infrared Spectra of Isotope-Substituted 4-(Dimethylamino)Benzonitriles and Molecular Structure of the Charge-Transfer Singlet Excited State. *J. Phys. Chem. A* **2001**, *105*, 4182−4188.

(16) Okamoto, H.; Kinoshita, M. Picosecond Infrared Spectrum of 4-(Pyrrol-1-Yl)Benzonitrile: Structure of the Excited Charge-Transfer States of Donor-Acceptor Systems. *J. Phys. Chem. A* **2002**, *106*, 3485−3490.

(17) Ma, C.; Kwok, W. M.; Matousek, P.; Parker, A. W.; Phillips, D.; Toner, W. T.; Towrie, M. Excited States of 4-Aminobenzonitrile (ABN) and 4-Dimethylaminobenzonitrile (DMABN): Time-Resolved Resonance Raman, Transient Absorption, Fluorescence, and Ab Initio Calculations. *J. Phys. Chem. A* **2002**, *106*, 3294−3305.

(18) Fuss, W.; Pushpa, K. K.; Rettig, W.; Schmid, W. E.; Trushin, S. A. Ultrafast Charge Transfer Via a Conical Intersection in Dimethylaminobenzonitrile. *Photochem. & Photobiol. Sci.* **2002**, *1*, 255−262.

(19) Yoshihara, T.; Galievsky, V. A.; Druzhinin, S. I.; Saha, S.; Zachariasse, K. A. Singlet Excited State Dipole Moments of Dual Fluorescent N-Phenylpyrroles and 4-(Dimethylamino)Benzonitrile from Solvatochromic and Thermochromic Spectral Shifts. *Photochem. & Photobiol. Sci.* **2003**, *2*, 342−353.

(20) Zachariasse, K. A.; Druzhinin, S. I.; Bosch, W.; Machinek, R. Intramolecular Charge Transfer with the Planarized 4-Aminobenzonitrile 1-Tert-Butyl-6-Cyano-1,2,3,4-Tetrahydroquinoline (NTC6). *J. Am. Chem. Soc.* **2004**, *126*, 1705−1715.

(21) Galievsky, V. A.; Zachariasse, K. A. Intramolecular Charge Transfer with N,N-Dialkyl-4-(Trifluoromethyl)Anilines and 4-(Dimethylamino)Benzonitrile in Polar Solvents. Investigation of the Excitation Wavelength Dependence of the Reaction Pathway. *Acta Phys. Pol., A* **2007**, *112*, S39−S56.

(22) Leinhos, U.; Kühnle, W.; Zachariasse, K. A. Intramolecular Charge-Transfer and Thermal Exciplex Dissociation with Para-Aminobenzonitriles in Toluene. *J. Phys. Chem.* **1991**, *95*, 2013−2021.

(23) Serrano-Andres, L.; Merchan, M.; Roos, B. O.; Lindh, R. Theoretical-Study of the Internal Charge-Transfer in Aminobenzonitriles. *J. Am. Chem. Soc.* **1995**, *117*, 3189−3204.

(24) Parusel, A. B. J.; Köhler, G.; Nooijen, H. A Coupled-Cluster Analysis of the Electronic Excited States in Aminobenzonitriles. *J. Phys. Chem. A* **1999**, *103*, 4056−4064.

(25) Sudholt, W.; Staib, A.; Sobolewski, A. L.; Domcke, W. Molecular-Dynamics Simulations of Solvent Effects in the Intramolecular Charge Transfer of 4-(N,N-Dimethylamino)Benzonitrile. *Phys. Chem. Chem. Phys.* **2000**, *2*, 4341−4353.

(26) Rappoport, D.; Furche, F. Photoinduced Intramolecular Charge Transfer in 4-(Dimethyl)Aminobenzonitrile - a Theoretical Perspective. *J. Am. Chem. Soc.* **2004**, *126*, 1277−1284.

(27) Köhn, A.; Hättig, C. On the Nature of the Low-Lying Singlet States of 4-(Dimethyl-Amino)Benzonitrile. *J. Am. Chem. Soc.* **2004**, *126*, 7399−7410.

(28) Amatatsu, Y. Theoretical Study on the Photochemical Behavior of 4-(Dimethylamino)Benzonitrile. *J. Phys. Chem. A* **2005**, *109*, 7225−7235.

(29) Gómez, I.; Reguero, M.; Boggio-Pasqua, M.; Robb, M. A. Intramolecular Charge Transfer in 4-Aminobenzonitriles Does Not Necessarily Need the Twist. *J. Am. Chem. Soc.* **2005**, *127*, 7119−7129.

(30) Gómez, I.; Mercier, Y.; Reguero, M. Theoretical Investigation of Luminescence Behavior as a Function of Alkyl Chain Size in 4-Aminobenzonitrile Alicyclic Derivatives. *J. Phys. Chem. A* **2006**, *110*, 11455−11461.

(31) Hättig, C.; Hellweg, A.; Köhn, A. Intramolecular Charge-Transfer Mechanism in Quinolidines: The Role of the Amino Twist Angle. *J. Am. Chem. Soc.* **2006**, *128*, 15672−15682.

(32) Minezawa, N.; Kato, S. Intramolecular Charge-Transfer State Formation of 4-(N,N-Dimethylamino)Benzonitrile in Acetonitrile Solution: RISM-SCF Study. *J. Phys. Chem. A* **2005**, *109*, 5445−5453.

(33) Mennucci, B.; Toniolo, A.; Tomasi, J. Ab Initio Study of the Electronic Excited States in 4-(N,N-Dimethylamino)Benzonitrile with Inclusion of Solvent Effects: The Internal Charge Transfer Process. *J. Am. Chem. Soc.* **2000**, *122*, 10621−10630.

(34) Scalmani, G.; Frisch, M. J.; Mennucci, B.; J, T. Geometries and Properties of Excited States in the Gas Phase and in Solution: Theory and Application of a Time-Dependent Density Functional Theory Polarizable Continuum Model. *J. Chem. Phys.* **2006**, *124*, 094107.

(35) Chiba, M.; Tsuneda, T.; Hirao, K. Long-Range Corrected Time-Dependent Density Functional Study on Fluorescence of 4,4′-Dimethylaminobenzonitrile. *J. Chem. Phys.* **2007**, *126*, 034504−11.

(36) Lee, J. K.; Fujiwara, T.; Kofron, W. G.; Zgierski, M. Z.; Lim, E. C. The Low-Lying $\pi\sigma^*$ State and Its Role in the Intramolecular Charge Transfer of Aminobenzonitriles and Aminobenzethyne. *J. Chem. Phys.* **2008**, *128*, 164512.

(37) Gustavsson, T.; Coto, P. B.; Serrano-Andres, L.; Fujiwara, T.; Lim, E. C. Do Fluorescence and Transient Absorption Probe the Same Intramolecular Charge Transfer State of 4-(Dimethylamino)-Benzonitrile? *J. Chem. Phys.* **2009**, *131*, 031101.

(38) Coto, P. B.; Serrano-Andres, L.; Gustavsson, T.; Fujiwara, T.; Lim, E. C. Intramolecular Charge Transfer and Dual Fluorescence of 4-(Dimethylamino) Benzonitrile: Ultrafast Branching Followed by a Two-Fold Decay Mechanism. *Phys. Chem. Chem. Phys.* **2011**, *13*, 15182−15188.

(39) Lunkenheimer, B.; Köhn, A. Solvent Effects on Electronically Excited States Using the Conductor-Like Screening Model and the Second-Order Correlated Method ADC(2). *J. Chem. Theory Comput.* **2013**, *9*, 977−994.

(40) Cogan, S.; Zilberg, S.; Haas, Y. The Electronic Origin of the Dual Fluorescence in Donor-Acceptor Substituted Benzene Derivatives. *J. Am. Chem. Soc.* **2006**, *128*, 3335−3345.

(41) Haas, Y.; Zilberg, S.; Dick, B. Conical Intersections and the Electronic Structure of the Excited States of N-Phenyl Pyrrole - A Prototype Molecule Exhibiting Dual Fluorescence. *Pol. J. Chem.* **2008**, *82*, 773−793.

(42) Kochman, M. A.; Tajti, A.; Morrison, C. A.; Miller, R. J. D. Early Events in the Nonadiabatic Relaxation Dynamics of 4-(N,N-Dimethylamino)Benzonitrile. *J. Chem. Theory Comput.* **2015**, *11*, 1118−1128.

(43) Druzhinin, S. I.; Mayer, P.; Stalke, D.; von Bulow, R.; Noltemeyer, M.; Zachariasse, K. A. Intramolecular Charge Transfer with 1-Tert-Butyl-6-Cyano-1,2,3,4-Tetrahydroquinoline (NTC6) and Other Aminobenzonitriles. A Comparison of Experimental Vapor Phase Spectra and Crystal Structures with Calculations. *J. Am. Chem. Soc.* **2010**, *132*, 7730−7744.

(44) Trushin, S. A.; Yatsuhashi, T.; Fuss, W.; Schmid, W. E. Coherent Oscillations in the Charge-Transfer System 4-Dimethylamino-Benzonitrile. *Chem. Phys. Lett.* **2003**, *376*, 282−291.

(45) Salgado, F. P.; Herbich, J.; Kunst, A. G. M.; Rettschnick, R. P. H. Structure and Picosecond Excited-States Dynamics in Isolated, Supercooled 4-(N,N-Dimethylamino)Benzonitrile. *J. Phys. Chem. A* **1999**, *103*, 3184−3192.

(46) Kwok, W. M.; Ma, C.; Matousek, P.; Parker, A. W.; Phillips, D.; Toner, W. T.; Towrie, M.; Umapathy, S. A Determination of the Structure of the Intramolecular Charge Transfer State of 4-Dimethylaminobenzonitrile (DMABN) by Time-Resolved Resonance Raman Spectroscopy. *J. Phys. Chem. A* **2001**, *105*, 984−990.

(47) Schirmer, J. Beyond the Random-Phase Approximation - a New Approximation Scheme for the Polarization Propagator. *Phys. Rev. A: At, Mol., Opt. Phys.* **1982**, *26*, 2395−2416.

(48) Hättig, C. Structure Optimizations for Excited States with Correlated Second-Order Methods: CC2 and ADC(2). *Adv. Quantum Chem.* **2005**, *50*, 37−60.

(49) Druzhinin, S. I.; Ernsting, N. P.; Kovalenko, S. A.; Lustres, L. W.; Senyushkina, T. A.; Zachariasse, K. A. Dynamics of Ultrafast Intramolecular Charge Transfer with 4-(Dimethylamino)Benzonitrile in Acetonitrile. *J. Phys. Chem. A* **2006**, *110*, 2955−2969.

(50) Galvan, I. F.; Martin, M. E.; Aguilar, M. A. On the Absorption Properties of the Excited States of DMABN. *Chem. Phys. Lett.* **2010**, *499*, 100−102.

(51) Szalay, P. G.; Müller, T.; Gidofalvi, G.; Lischka, H.; Shepard, R. Multiconfiguration Self-Consistent Field and Multireference Configuration Interaction Methods and Applications. *Chem. Rev.* **2012**, *112*, 108−181.

(52) Klamt, A.; Schüürmann, G. Cosmo - a New Approach to Dielectric Screening in Solvents with Explicit Expressions for the Screening Energy and Its Gradient. *J. Chem. Soc., Perkin Trans. 2* **1993**, 799−805.

(53) Klamt, A. The COSMO and COSMO-Rs Solvation Models. *Wires Comput. Mol. Sci.* **2011**, *1*, 699−709.

(54) Møller, C.; Plesset, M. S. Note on an Approximation Treatment for Many-Electron Systems. *Phys. Rev.* **1934**, *46*, 618−622.

(55) Schäfer, A.; Horn, H.; Ahlrichs, R. Fully Optimized Contracted Gaussian-Basis Sets for Atoms Li to Kr. *J. Chem. Phys.* **1992**, *97*, 2571−2577.

(56) Pople, J. A.; Seeger, R.; Krishnan, R. Variational Configuration Interaction Methods and Comparison with Perturbation-Theory. *Int. J. Quantum Chem.* **1977**, *12* (S11), 149−163.

(57) Pierloot, K.; Dumez, B.; Widmark, P. O.; Roos, B. O. Density-Matrix Averaged Atomic Natural Orbital (Ano) Basis-Sets for Correlated Molecular Wave-Functions 0.4. Medium-Size Basis-Sets for the Atoms H-Kr. *Theor. Chim. Acta* **1995**, *90*, 87−114.

(58) Klamt, A. Calculation of UV/Vis Spectra in Solution. *J. Phys. Chem.* **1996**, *100*, 3349−3353.

(59) do Monte, S. A.; Müller, T.; Dallos, M.; Lischka, H.; Diedenhofen, M.; Klamt, A. Solvent Effects in Electronically Excited States Using the Continuum Solvation Model COSMO in Combination with Multireference Configuration Interaction with Singles and Doubles (MR-CISD). *Theor. Chem. Acc.* **2004**, *111*, 78−89.

(60) Shepard, R.; Lischka, H.; Szalay, P. G.; Kovar, T.; Ernzerhof, M. A General Multireference Configuration-Interaction Gradient Program. *J. Chem. Phys.* **1992**, *96*, 2085−2098.

(61) Lischka, H.; Dallos, M.; Shepard, R. Analytic MRCI Gradient for Excited States: Formalism and Application to the n-π* Valence- and n-(3s,3p) Rydberg States of Formaldehyde. *Mol. Phys.* **2002**, *100*, 1647−1658.

(62) Lischka, H.; Dallos, M.; Szalay, P. G.; Yarkony, D. R.; Shepard, R. Analytic Evaluation of Nonadiabatic Coupling Terms at the MR-CI Level. I. Formalism. *J. Chem. Phys.* **2004**, *120*, 7322−7329.

(63) Dallos, M.; Lischka, H.; Shepard, R.; Yarkony, D. R.; Szalay, P. G. Analytic Evaluation of Nonadiabatic Coupling Terms at the MR-CI Level. II. Minima on the Crossing Seam: Formaldehyde and the Photodimerization of Ethylene. *J. Chem. Phys.* **2004**, *120*, 7330−7339.

(64) Ahlrichs, R.; Weigend, F.; Häser, M.; Patzelt, H. RI-MP2: Optimized Auxiliary Basis Sets and Demonstration of Efficiency. *Chem. Phys. Lett.* **1998**, *294*, 143−152.

(65) Lischka, H.; Shepard, R.; Pitzer, R. M.; Shavitt, I.; Dallos, M.; Muller, T.; Szalay, P. G.; Seth, M.; Kedziora, G. S.; Yabushita, S.; Zhang, Z. Y. High-Level Multireference Methods in the Quantum-Chemistry Program System Columbus: Analytic MR-CISD and MR-AQCC Gradients and MR-AQCC-LRT for Excited States, GUGA Spin-Orbit CI and Parallel CI Density. *Phys. Chem. Chem. Phys.* **2001**, *3*, 664−673.

(66) Lischka, H.; Müller, T.; Szalay, P. G.; Shavitt, I.; Pitzer, R. M.; Shepard, R. Columbus-a Program System for Advanced Multireference Theory Calculations. *Wires Comput. Mol. Sci.* **2011**, *1*, 191−199.

(67) Dachsel, H.; Lischka, H.; Shepard, R.; Nieplocha, J.; Harrison, R. J. A Massively Parallel Multireference Configuration Interaction Program: The Parallel Columbus Program. *J. Comput. Chem.* **1997**, *18*, 430−448.

(68) Müller, T. Large-Scale Parallel Uncontracted Multireference-Averaged Quadratic Coupled Cluster: The Ground State of the Chromium Dimer Revisited. *J. Phys. Chem. A* **2009**, *113*, 12729−12740.

(69) Heine, A.; Herbstirmer, R.; Stalke, D.; Kuhnle, W.; Zachariasse, K. A. Structure and Crystal Packing of 4-Aminobenzonitriles and 4-Amino-3,5-Dimethylbenzonitirles at Various Temperatures. *Acta Crystallogr., Sect. B: Struct. Sci.* **1994**, *50*, 363−373.

(70) Kajimoto, O.; Yokoyama, H.; Ooshima, Y.; Endo, Y. The Structure of 4-(N,N-Dimethylamino)Benzonitrile and Its Vanderwaals Complexes. *Chem. Phys. Lett.* **1991**, *179*, 455−459.

(71) Blake, A. J.; Ebsworth, E. A. V.; Welch, A. J. Structure of Trimethylamine, C3H9N, at 118-K. *Acta Crystallogr., Sect. C: Cryst. Struct. Commun.* **1984**, *40*, 413−415.

(72) Grassian, V. H.; Warren, J. A.; Bernstein, E. R.; Secor, H. V. Conformational-Changes Upon S1-S0 Excitation in 4-Dimethylaminobenzonitrile and Some of Its Chemical Analogs. *J. Chem. Phys.* **1989**, *90*, 3994−3999.

(73) Saigusa, H.; Miyakoshi, N.; Mukai, C.; Fukagawa, T.; Kohtani, S.; Nakagaki, R.; Gordon, R. Twisted S-1 Excited State Geometries in 4-Dimethylaminobenzonitrile and Dimethylaniline: New -D(6) Origin Bands. *J. Chem. Phys.* **2003**, *119*, 5414−5422.

(74) Nikolaev, A. E.; Myszkiewicz, G.; Berden, G.; Meerts, W. L.; Pfanstiel, J. F.; Pratt, D. W. Twisted Intramolecular Charge Transfer States: Rotationally Resolved Fluorescence Excitation Spectra of 4,4′-Dimethylaminobenzonitrile in a Molecular Beam. *J. Chem. Phys.* **2005**, *122*, 084309.

(75) Rhinehart, J. M.; Mehlenbacher, R.; McCamant, D. W. Photoinduced Structural Dynamics of 4-(Dimethylamino)Benzonitrile (DMABN) Probed with Femtosecond Stimulated Raman Spectroscopy. *AIP Conf. Proc.* **2010**, *1267*, 39−40.

(76) Galvan, I. F.; Martin, M. E.; Aguilar, M. A. Theoretical Study of the Dual Fluorescence of 4-(N,N-Dimethylamino)Benzonitrile in Solution. *J. Chem. Theory Comput.* **2010**, *6*, 2445−2454.

(77) Schuddeboom, W.; Jonker, S. A.; Warman, J. M.; Leinhos, U.; Kuhnle, W.; Zachariasse, K. A. Excited-State Dipole-Moments of Dual Fluorescent 4-(Dialkylamino)Benzonitriles - Influence of Alkyl Chain-Length and Effective Solvent Polarity. *J. Phys. Chem.* **1992**, *96*, 10809−10819.

(78) Baumann, W.; Bischof, H.; Frohling, J. C.; Brittinger, C.; Rettig, W.; Rotkiewicz, K. Considerations on the Dipole-Moment of Molecules Forming the Twisted Intramolecular Charge-Transfer State. *J. Photochem. Photobiol., A* **1992**, *64*, 49−72.

(79) Mulliken, R. S. Electronic Population Analysis on LCAO MO Molecular Wave Functions. *J. Chem. Phys.* **1955**, *23*, 1833−1840.

(80) Yarkony, D. R. Conical Intersections: Diabolical and Often Misunderstood. *Acc. Chem. Res.* **1998**, *31*, 511−518.

(81) Atchity, G. J.; Xantheas, S. S.; Ruedenberg, K. Potential-Energy Surfaces near Intersections. *J. Chem. Phys.* **1991**, *95*, 1862−1876.

(82) Domcke, W.; Yarkony, D. R.; Köppel, H. *Conical Intersections: Electronic Structure, Dynamics & Spectroscopy*; World Scientific: River Edge, NJ, 2004.

(83) Zgierski, M. Z.; Lim, E. C. Electronic and Vibrational Spectra of the Low-Lying $\pi\sigma$* State of 4-Dimethylaminobenzonitrile: Comparison of Theoretical Predictions with Experiment. *J. Chem. Phys.* **2005**, *122*, 111103.